Available online at www.sciencedirect.com
SciVerse ScienceDirect
Ceramics International 38 (2012) 1473–1477
CERAMICS INTERNATIONAL
www.elsevier.com/locate/ceramint

Influence of manganese on the structure and magnetic properties of $YFeO_3$ nanocrystal

Hui Shen [a,*], Jiayue Xu [a,b], Min Jin [a], Guojian Jiang [a]

[a] *School of Materials Science and Engineering, Shanghai Institute of Technology, Shanghai 200235, PR China*
[b] *Shanghai Institute of Ceramics, Chinese Academy of Sciences, Shanghai 200050, PR China*

Received 22 July 2011; received in revised form 28 August 2011; accepted 13 September 2011
Available online 17 September 2011

Abstract

High purity Mn doped $YFeO_3$ nanocrystals were readily prepared by sol–gel combustion method, with citric acid as the fuel. The doping effect on the structure and magnetic properties was systematically studied. X-ray diffraction and TEM results indicate that the samples are well crystallized. Orthorhombic $YFeO_3$ crystallites can be obtained when calcined at 800 °C. In $YFe_{1-x}Mn_xO_3$ system for $x \leq 0.2$, hexagonal structure exists as metastable phase and the calcined temperature has to be elevated to obtain pure orthorhombic phase. Distortion of the crystal structure was also observed, with changes in lattice parameters. The antiferromagnetic coupling was effectively strengthened with increased Mn content. This is possibly originated from the structural distortion which gives rise to enhanced antiferromagnetic superexchange interaction between Fe^{3+}–Fe^{3+} and Fe^{3+}–Mn^{3+}.

Keywords: D. Perovskites; Nanocrystals; Combustion method

1. Introduction

Orthoferrites of formula $RFeO_3$ (R = Y and rare earth) are a family of compounds showing a variety of interesting physical and chemical properties. First, $RFeO_3$ single crystal displays unique magnetic and magneto-optical properties, with promising advantages in innovative magnetic and optical devices in the fields of ultrafast optical switches, light spot position measurements and magneto-optical current sensor [1–3]. Second, nanocrystalline $RFeO_3$ is required for several technological applications and synthesis of nano-scaled materials is gaining tremendous interest, since $RFeO_3$ powder with ultra small dimensions usually exhibit superior properties, such as improved catalytic properties for water decomposition [4,5]. They also show promising applications in the fields of solid-oxide fuel cells (SOFCs), chemical sensors and semiconductors, etc. [6].

$RFeO_3$ crystallizes in orthorhombic perovskite-type structure, and shows unique magnetic properties. Doping with transition metals has been proved to be very effective in improving magnetic and ferroelectric properties of $YMnO_3$ and $BiFeO_3$ which crystallize in similar structure and are also important magnetic and multiferroic compounds [7,8]. For example, transition metal (Mn, Cr) doped $BiFeO_3$ shows significant enhancement in their magnetic moment. Therefore, the magnetic properties of $YFeO_3$ are also expected to be effectively modified by the transition metal doping, which will explore its applications for important technological innovations.

In this work, a series of Mn doped $YFeO_3$ nanocrystals was prepared by sol–gel combustion method. This method is an easy and convenient method for the preparation of a variety of nanomaterials [9]. Although there are a variety of orthoferrites compounds with different rare earths, $YFeO_3$ was selected because there is no magnetic rare-earth ion in $YFeO_3$. So only the interactions between Fe and Mn ions have to be taken into account. A systematic study of the doping effects on the structure and magnetic properties of $YFeO_3$ was carried out.

2. Experiments

$YFe_{1-x}Mn_xO_3$ ($x = 0$, 0.05, 0.1, 0.15, 0.2) nano-powders were prepared by sol–gel combustion method. Rare earth oxide Y_2O_3 (99.99% purity), $Fe(NO_3)_3{\cdot}9H_2O$, $Mn(NO_3)_2{\cdot}4H_2O$ and

* Corresponding author. Tel.: +86 21 64941205; fax: +86 21 64941205.
E-mail address: hshen@sit.edu.cn (H. Shen).

0272-8842/$36.00
doi:10.1016/j.ceramint.2011.09.030

citric acid (AR) were used as raw materials. An aqueous nitrate solution of Y^{3+} was prepared by dissolving Y_2O_3 in diluted in nitric acid (HNO_3, AR) under stirring at 60 °C for 2 h. $Fe(NO_3)_3 \cdot 9H_2O$ and $Mn(NO_3)_2 \cdot 4H_2O$ were also dissolved in distilled water and mixed with the rare earth nitrates in stoichiometric ratio of Y:Fe = 1:1. Citric acid was then added as a fuel to the above solution to yield a citrate–nitrite ratio of 1.0–1.5. The pH value of the solution was adjusted to 1–2 by adding small amount of aqua ammonia solution. The mixed solution was continuously stirred using a magnetic agitator. The solution was evaporated by heating at 85 °C until brown sticky gel was formed. Subsequently, the gel was ignited by increasing the temperature up to 300 °C. The dried gel burnt in a self-propagating combustion manner and large volume of brown fume evolved. Finally, a voluminous porous powder was obtained and the powder was calcined at different temperatures in air for 2 h.

Phase identification was checked by powder X-ray diffraction (XRD, D/Max-2550V, Rigaku, Japan) using Cu Kα radiation and nickel as the filter. The morphology and particle size of the heat-treated powder were examined by transmission electronic microscopy (TEM, H-800, Hitachi, Japan). The magnetic measurements of the samples were performed on a superconducting quantum interference device magnetometer (Quantum design, PPMS-9).

3. Results and discussion

When the dried gel samples were ignited, the combustion rapidly propagated until all samples burnt out completely and formed an aggregate of loose powders with a large amount of microscopic pores. In the self-combustion process, citric acid is served as the fuel and is oxidized by the nitrates. The citric acid to metal nitrates molar ratio (CA/MN) has a strong effect on the reaction temperature and the phase structure. In order to evaluate the effect of CA/MN on the combustion behavior, CA/MN molar ratio of 1 and 1.5 has been chosen. From the XRD patterns in Fig. 1, it can be observed that as-burnt sample at ratio of 1.5 exists in an amorphous form, while distinct diffraction peaks were observed for the sample synthesized at ratio of 1. It proves that the excessive amount of fuels does not favor complete self-combustion reaction.

Fig. 1 also shows the XRD patterns of as-burnt and calcined $YFeO_3$ powders at different temperatures for 2 h, with the CA/MN molar ratio of 1. The as-burnt powders have already crystallized, indicating that the self-propagating process was complete and almost all the organic compounds have been burnt out. The diffraction peaks of as-burnt powders correspond to the mixture of hexagonal and orthorhombic $YFeO_3$ (JCPDS No. 48-0529, 39-1489). When the samples were calcined at 700 °C for 2 h, the two phases were still observed, with increased diffraction intensity. Pure orthorhombic $YFeO_3$ was successfully obtained when the calcined temperature increased to 800 °C, as seen in Fig. 1(d). Metastable $YFeO_3$ with hexagonal structure, space group *P*63/*mmc*, was also obtained by other synthetic methods, such as thermal decomposition of $Y[Fe(CN)_6] \cdot 4H_2O$[10]. It also transforms to the orthorhombic structure at elevated temperatures.

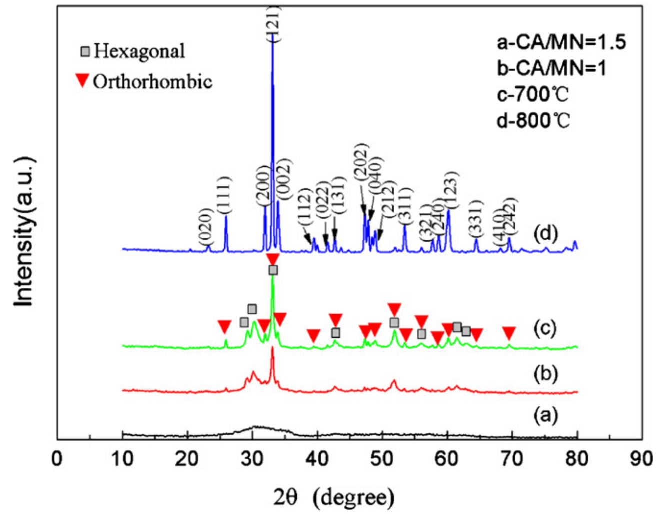

Fig. 1. XRD patterns of $YFeO_3$ powders calcined at different temperatures.

Fig. 2 shows the XRD patterns of the calcined powder with different Mn contents. All of them were synthesized by the same procedures and are calcined at 800 °C for 2 h. For the samples with Mn content less than 0.2, they are mixture of hexagonal and orthorhombic structure. However, the diffraction intensity of hexagonal $YFeO_3$ becomes gradually stronger with higher Mn content. Especially for $YFe_{0.8}Mn_{0.2}O_3$, the phase is only hexagonal at 800 °C, as seen in Fig. 2. The structure of $YMnO_3$ is different from that of $YFeO_3$. Thermodynamically, hexagonal $YMnO_3$ is more stable than the orthorhombic structure [11]. So in the $YFe_{1-x}Mn_xO_3$ system ($x \leq 0.2$), the diffraction intensity of hexagonal structure increased with Mn content.

The calcined temperatures were increased to obtain pure orthorhombic structure for Mn doped samples. And the optimized calcined temperatures for $YFe_{1-x}Mn_xO_3$ ($x = 0.05$,

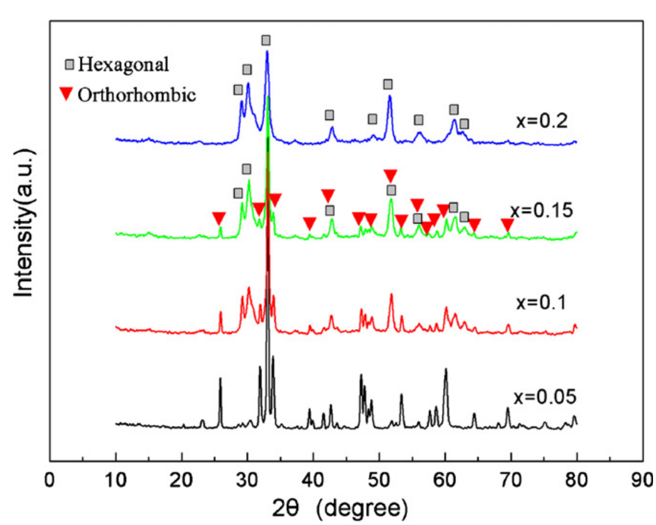

Fig. 2. XRD patterns of $YFe_{1-x}Mn_xO_3$ powders calcined at 800 °C for 2 h ($x = 0.05$, 0.1, 0.15, 0.2).

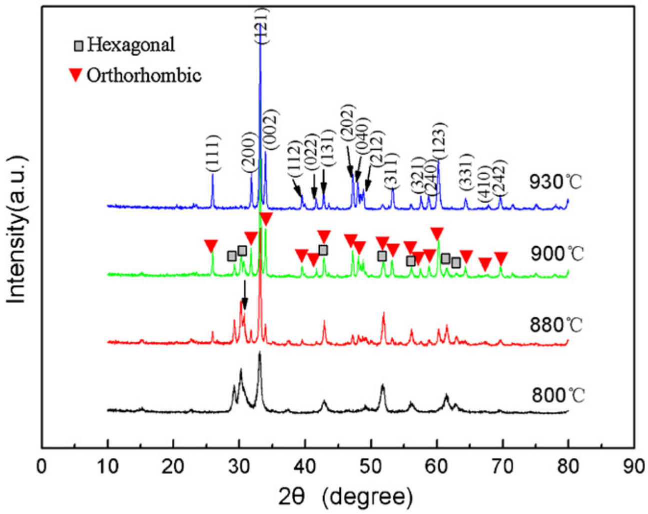

Fig. 3. XRD patterns of $YFe_{0.8}Mn_{0.2}O_3$ powders calcined at different temperatures.

0.1, 0.15, 0.2) are 820 °C, 850 °C, 880 °C and 930 °C. XRD analysis confirms that they are single phases with the orthorhombic structure (not shown here). The structural mismatch prevented $YFeO_3$ and $YMnO_3$ from forming a complete solid solution in the entire compositional region [12]. In particular, the XRD patterns of $YFe_{0.8}Mn_{0.2}O_3$ powders calcined at different temperatures are shown in Fig. 3. The intensity of hexagonal structure decreased gradually with elevated temperature, and orthorhombic structure was finally achieved when the temperature increased to 930 °C. Splitting of (1 0 1) peak, pointed by the arrow, was observed in the sample at 880 °C and 900 °C. Since no extra peaks were observed, it is assumed that the peak splitting is due to structural distortion rather than an impurity phase.

The lattice parameters *a*, *b* and *c* of these compounds were calculated from the diffraction data, which was determined by Jade software (version 6.5). As seen in Table 1, lattice parameter along *b* direction monotonically increases with increasing *x* whereas lattice parameters along *a* and *c* direction decrease. The change in the lattice constants suggests that the substitution of Mn induces a distortion in the crystal structure of $YFeO_3$. The tolerance factor (t) was used to distinguish the perovskite-type structures. The Goldschmidt tolerance factor (t) for perovskite can be calculated as follows using the ionic radii of large (r_A) and small (r_B) cations and (r_O) of anions [13]:

$$t = \frac{r_A + r_O}{\sqrt{2}(r_B + r_O)} \quad (1)$$

For Mn doped $YFeO_3$ system, the tolerance factors can be calculated by the following relationship:

$$t = \frac{r_Y + r_O}{\sqrt{2}[(1-x)r_{Fe} + xr_{Mn} + r_O]} \quad (2)$$

The ideal cubic perovskite corresponds to $t = 1$, and the factor adjusts to $t < 1$ for orthorhombic structure. The radius of Mn^{3+} is larger than that of Fe^{3+}, so the Fe–O bond distance increases with the increase of manganese content [12]. According to Eq. (2), the tolerance factor decreased with the increase of Mn content in $YFe_{1-x}Mn_xO_3$. The magnitude of tilting increases with the decrease of the tolerance factors [14]. So it implies that the magnitude of tilting of FeO_6 octahedral increases with increasing Mn content. In orthorhombic perovskite structure, FeO_6 octahedra rotated around the orthorhombic *b*-axis, resulting in tilted FeO_6 octahedra [12]. When more Mn was introduced, the FeO_6 octahedron tilted more around the *b*-axis. So lattice parameter of *b* increases, and lattice parameters *a* and *c* decrease.

Table 1
Lattice parameters of Mn doped $YFeO_3$ nanocrystals.

Compound	*a* (Å)	*b* (Å)	*c* (Å)
$YFeO_3$	5.28651	5.59476	7.61002
$YFe_{0.95}Mn_{0.05}O_3$	5.27985	5.59738	7.59786
$YFe_{0.9}Mn_{0.1}O_3$	5.27889	5.60545	7.58984
$YFe_{0.85}Mn_{0.15}O_3$	5.27865	5.61609	7.57585
$YFe_{0.8}Mn_{0.2}O_3$	5.27738	5.62040	7.56148

The morphology of these orthorhombic nano-powders was investigated by TEM. Fig. 4 presents typical TEM images of the orthorhombic powders with compositions of $YFeO_3$, $YFe_{0.9}Mn_{0.1}O_3$ and $YFe_{0.8}Mn_{0.2}O_3$. All the samples were well crystallized and the grain boundaries are clearly distinguishable. The average grain size of these samples slightly increases with Mn content, which is possibly attributed to the higher calcined temperature. The crystallites of pure $YFeO_3$ powder agglomerated forming grains of about 50 nm in diameter. The average size of $YFe_{0.9}Mn_{0.1}O_3$ and $YFe_{0.8}Mn_{0.2}O_3$ is estimated to be around 70 nm and 90 nm, respectively.

Magnetic properties of orthorhombic $YFeO_3$ nanocrystals with varied Mn content were investigated by PPMS, which are shown in Fig. 5. The undoped $YFeO_3$ nanopowder displays obvious hysteretic loop, indicating ferromagnetic behavior. Its magnetization reached 0.015 emu/g at 60 kOe, and still has the tendency to increase. The coercive field (Hc) is about 35 kOe. For $YFe_{0.9}Mn_{0.1}O_3$ and $YFe_{0.8}Mn_{0.2}O_3$ samples, their magnetic moments have increased, reaching 0.08 emu/g at 6000 Oe, but the remnant magnetization (Mr) and coercive field decreased greatly with increased Mn contents. The Mr is only 0.005 emu/g and the Hc reduced to 273 Oe for $YFe_{0.9}Mn_{0.1}O_3$ nanocrystal. Linear *M–H* curve was observed for $YFe_{0.8}Mn_{0.2}O_3$ nanocrystal, with almost zero Hc and Mr. The behavior is typical antiferromagnetic, which is significantly different from that of pure $YFeO_3$.

The magnetic moments of iron and rare earth atoms as well as the interactions between them are the source of the interesting magnetic coupling of the $RFeO_3$ family. Since Y^{3+} is non-magnetic, the magnetic interaction Y^{3+} between Fe^{3+} is absent in $YFeO_3$. $YFeO_3$ crystallizes in distorted perovskite structure with an orthorhombic unit cell. The FeO_6 octahedra are tilted to several degrees due to the low symmetry of orthorhombic structure. Correspondingly, the magnetic lattice is comprised of collinear antiferromagnetic spin order along a particular crystallographic direction and a canted spin order which gives rise to weak ferromagnetism [15,16].

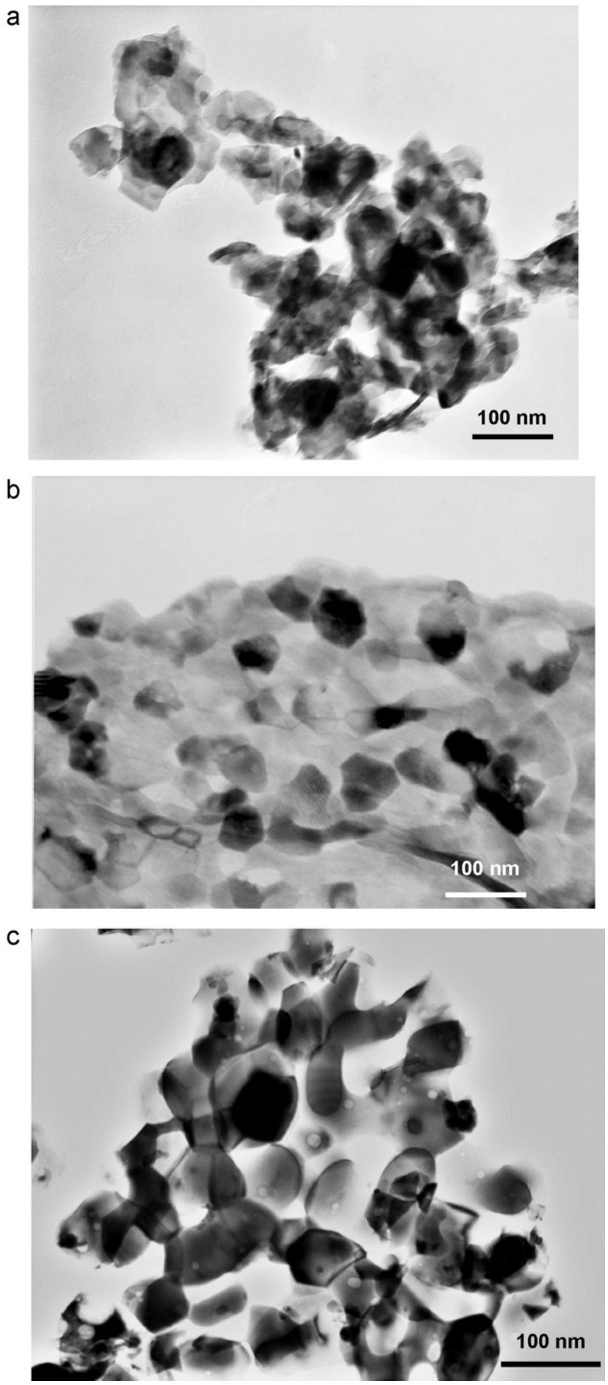

Fig. 4. TEM images of nano powders: (a) $YFeO_3$, (b) $YFe_{0.9}Mn_{0.1}O_3$ and (c) $YFe_{0.8}Mn_{0.2}O_3$.

The magnetic moment of the Mn^{3+} ion is thought to be larger than that of Fe^{3+} in the perovskite-type oxides, and this must be the reason why the magnetic moments increase with higher Mn content in Mn doped $YFeO_3$ system [15]. Interestingly, enhancements of the antiferromagnetic ordering by the Mn substitution were also observed. The distortion in the crystal structure was induced through Mn^{3+} substitution for Fe^{3+} in $YFeO_3$. It is suggested that the bond angle of Fe–O–Fe in ab plane increases with increasing Mn content. The increase in the bond angle may enhance antiferromagnetic superexchange interaction between Fe^{3+}–Fe^{3+} and Fe^{3+}–Mn^{3+}, resulting in increased antiferromagnetic coupling [17].

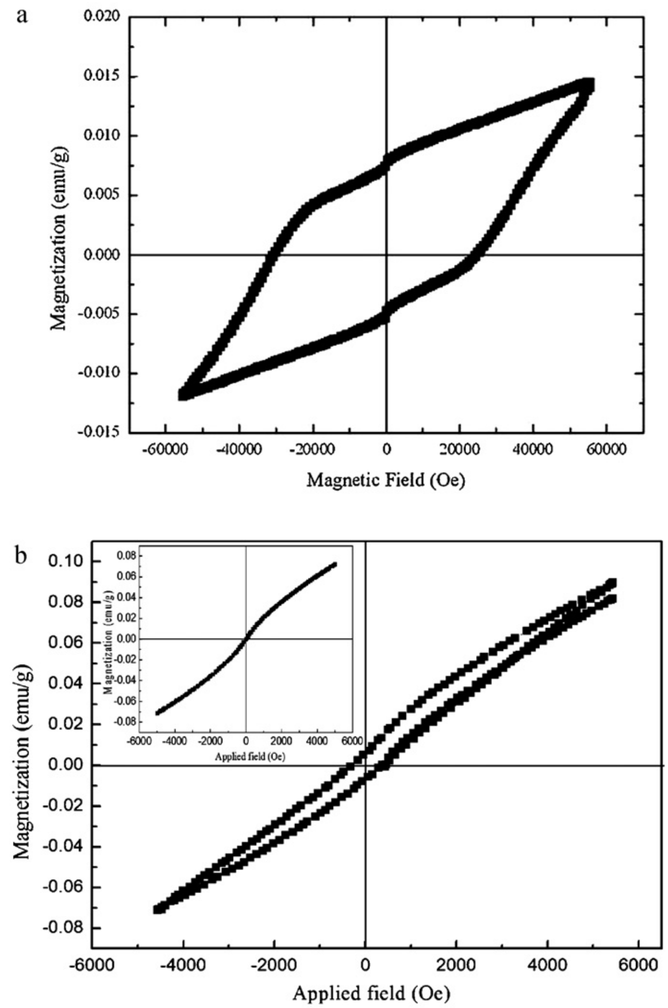

Fig. 5. Room temperature hysteresis curves of nano powders: (a) $YFeO_3$, (b) $YFe_{0.9}Mn_{0.1}O_3$, inset: the *M–H* loop of $YFe_{0.8}Mn_{0.2}O_3$.

4. Conclusions

The synthesis of $YFe_{1-x}Mn_xO_3$ ($x \leq 0.2$) nanocrystals was readily conducted by sol–gel combustion method. Orthorhombic structure is the stable phase in these compounds with $x \leq 0.2$, although the hexagonal structure exists as metastable phase in Mn doped $YFeO_3$ system. It was found that elevated calcined temperature is needed in order to obtain pure orthorhombic structure. Mn doping also resulted in the distortion of crystal structure, and its magnetic behavior was modified, correspondingly. Compared with the undoped $YFeO_3$, the magnetic moments became larger, and the antiferromagnetic interactions were enhanced in Mn doped nanocrystals.

Acknowledgements

The authors would like to acknowledge the financial support provided by National Natural Science Foundation of China

(Nos. 51002097 and 50972093), Shanghai Science and Technology Committee (No. 10XD1403800) and the Shanghai Education Commission (Nos. 11YZ223, 10ZZ127, 09ZZ196 and J51504).

References

[1] Y.S. Didosyan, H. Hauser, G.A. Raider, W. Toriser, Fast latching type optical switch, J. Appl. Phys. 95 (2004) 7339.
[2] Y.S. Didosyan, H. Hauser, J. Nicolics, Magneto-optical current sensors of high bandwidth, Sens. Actuators 81 (2000) 263.
[3] H. Shen, J.Y. Xu, A.H. Wu, J.T. Zhao, M.L. Shi, Magnetic and thermal properties of perovskite $YFeO_3$ single crystal, Mater. Sci. Eng. B 157 (2009) 77.
[4] K.M. Parida, K.H. Reddy, S. Matha, D.P. Das, N. Biswal, Fabrication of nanocrystalline $LaFeO_3$: an efficient sol–gel auto-combustion assisted visible light responsive photocatalyst for water decomposition, Int. J. Hydrogen Energy 35 (2010) 12161–12168.
[5] H. Xu, X.L. Hu, L.Z. Zhang, Generalized low-temperature synthesis of nanocrystalline rare-earth orthoferrites $LnFeO_3$ (Ln = La, Pr, Nd, Sm, Eu, Gd), Cryst. Growth Des. 8 (2008) 2061–2065.
[6] R. Maiti, S. Basu, D. Chakravorty, Synthesis of nanocrystalline $YFeO_3$ and its magnetic properties, J. Magn. Magn. Mater. 321 (2009) 3274–3277.
[7] M. Zaghrioui, J.M. Greneche, C. Autret-Lambert, M. Gervais, Effect of Fe substitution on multiferroic hexagonal $YMnO_3$, J. Magn. Magn. Mater. 323 (2011) 509–514.
[8] Z.X. Cheng, X.L. Wang, Y. Du, S.X. Dou, A way to enhance the magnetic moment of multiferroic bismuth ferrite, J. Phys. D: Appl. Phys. 43 (2010), 242001, 5 pp.@@.
[9] F. Deganello, G. Marci, G. Deganello, Citrate–nitrate auto-combustion synthesis of perovskite-type nanopowders: a systematic approach, J. Eur. Ceram. Soc. 29 (2009) 439–450.
[10] D.M. Gil, M.C. Navarro, M.C. Lagarrigue, J. Guimpel, R.E. Carbonio, M.I. Gomez, Synthesis and structural characterization of perovskite $YFeO_3$ by the thermal decomposition of a cyano complex precursor $Y[Fe(CN)_6]\cdot 4H_2O$, J. Therm. Anal. Calorim. 103 (2011) 889.
[11] Y. Chen, H.M. Yuan, G.H. Li, G. Tian, S.H. Feng, Crystal growth and magnetic property of orthorhombic $RMnO_3$ (R = Sm–Ho) perovskites by mild hydrothermal synthesis, J. Cryst. Growth 305 (2007) 242–248.
[12] X.Q. Cao, C.S. Kim, H.Ill. Yoo, Effect of substitution of manganese for iron on the structure and electrical properties of yttrium ferrite, J. Am. Ceram. Soc. 84 (2001) 1265–1272.
[13] K. Ramam, K. Chandramouli, Dielectric and piezoelectric properties of rare-earth gadolinium modified lead lanthanum zirconium niobium titanate ceramics, Ceram. Int. 37 (2011) 979–984.
[14] F. Zhao, Z.X. Yue, Y.C. Zhang, Z.L. Gui, L.T. Li, Microstructure and microwave dielectric properties of $Ca[Ti_{1-x}(Mg_{1/3}Nb_{2/3})_x]O_3$ ceramics, J. Eur. Ceram. Soc. 25 (2005) 3347–3352.
[15] Y. Ma, Y.J. Wu, Y.Q. Lin, X.M. Chen, Microstructures and multiferroic properties of $YFe_{1-x}Mn_xO_3$ ceramics prepared by spark plasma sintering, J. Mater. Sci: Mater. Electron. 21 (2010) 838–843.
[16] H. Shen, J.Y. Xu, A.H. Wu, Preparation and characterization of perovskite $REFeO_3$ nanocrystalline powders, J. Rare Earths 28 (2010) 416–419.
[17] Y. Nagata, S. Yashiro, T. Mitsuhashi, A. Koriyama, Y. Kawashima, H. Samata, Magnetic properties of $RFe_{1-x}Mn_xO_3$ (R = Pr, Gd, Dy), J. Magn. Magn. Mater. 237 (2001) 250–260.